Enhanced Energy Expenditure, Glucose Utilization, and Insulin Sensitivity in VAMP8 Null Mice

Haihong Zong,[1] Cheng-Chun Wang,[2] Bhavapriya Vaitheesvaran,[1] Irwin J. Kurland,[1] Wanjin Hong,[2] and Jeffrey E. Pessin[1]

OBJECTIVE—Previous studies have demonstrated that the VAMP8 protein plays a complex role in the control of granule secretion, transport vesicle trafficking, phagocytosis, and endocytosis. The present study was aimed to investigate the role of VAMP8 in mediating GLUT4 trafficking and therefore insulin action in mice.

RESEARCH DESIGN AND METHODS—Physiological parameters were measured using Oxymax indirect calorimetry system in 12-week-old VAMP8 null mice. Dynamic analysis of glucose homeostasis was assessed using euglycemic–hyperinsulinemic clamp coupled with tracer radioactively labeled 2-deoxyglucose. Insulin stimulated GLUT4 protein expressions on muscle cell surface were examined by immunofluorescence microscopy.

RESULTS—VAMP8 null mice display reduced adiposity with increased energy expenditure despite normal food intake and reduced spontaneous locomotor activity. In parallel, the VAMP8 null mice also had fasting hypoglycemia (84 ± 11 vs. 115 ± 4) and enhanced glucose tolerance with increased insulin sensitivity due to increases in both basal and insulin-stimulated glucose uptake in skeletal muscle (0.19 ± 0.04 vs. 0.09 ± 0.01 mmol/kg/min during basal, 0.6 ± 0.04 vs. 0.31 ± 0.06 mmol/kg/min during clamp in red-gastrocnemius muscle, $P < 0.05$). Consistent with a role for VAMP8 in the endocytosis of the insulin-responsive GLUT4, sarcolemma GLUT4 protein levels were increased in both the basal and insulin-stimulated states without any significant change in the total amount of GLUT4 protein or related facilitative glucose transporters present in skeletal muscle, GLUT1, GLUT3, and GLUT11.

CONCLUSIONS—These data demonstrate that, in the absence of VAMP8, the relative subcellular distribution of GLUT4 is altered, resulting in increased sarcolemma levels that can account for increased glucose clearance and insulin sensitivity. ***Diabetes*** **60:30–38, 2011**

Insulin-stimulated glucose uptake in muscle and adipose tissue is mediated by the insulin-responsive GLUT isoform GLUT4 (1). In the basal state, ~95% of the GLUT4 protein is sequestered in intracellular membranes (termed the insulin-responsive storage vesicles) and after acute insulin stimulation undergoes a translocation process such that 50% of the GLUT4 protein is cell surface localized (2–5). There is now good evidence that vesicle fusion reactions are initiated by interactions among SNARE proteins (soluble *N*-ethylmaleimide-sensitive factor attachment protein receptors) that assemble into a four-helix bundle between the transport and acceptor membranes (6–8). It is generally accepted that the plasma membrane t-SNARE is composed of syntaxin 4 and SNAP23 whereas the v-SNARE present in GLUT4 vesicles is VAMP2 (9–15), although a recent study has suggested that several VAMP proteins can play redundant roles in this process (16). Endobrevin or VAMP8 was originally identified as an endosomal v-SNARE that mediated the homotypic fusion of early and late endosomes (13,17–21). Subsequently, VAMP8 was found to be present on several membrane compartments including early and late endosomes as well as the plasma membrane, *trans*-Golgi network, clathrin-coated pits, and secretory granules (15,19,22,23). VAMP8 was found to be required for mast cell degranulation, zymogen granule release from pancreatic acinar cells, and dense core granule release from platelets, suggesting that VAMP8 functions in plasma membrane exocytosis (13,19,24–28). On the other hand, it has been recently reported that VAMP8 functions to inhibit phagocytosis in immature dendritic cells, to induce membrane ruffles and bacterial entry into nonphagocytic cells, and for the efficient endocytosis of the plasma membrane GLUT4 protein in adipocytes (16,29). Thus, VAMP8 appears to have several functions that may be dependent upon the particular cell type and/or trafficking cargo material.

To further investigate the role of VAMP8, we have taken advantage of the VAMP8 null mouse (19) to examine the integrative physiology of glucose metabolism and GLUT4 trafficking in skeletal muscle in vivo. These data demonstrate that VAMP8 plays multiple roles in the whole-body regulation of metabolism, energy expenditure, and insulin sensitivity. Consistent with a role of VAMP8 in mediating GLUT4 endocytosis, skeletal muscle sarcolemma levels of GLUT4 were elevated in the VAMP8 null mice, directly accounting for the increase in both basal and insulin-stimulated glucose uptakes.

RESEARCH DESIGN AND METHODS

Animals. The control and VAMP8 knockout mice were maintained in a mixed C57BL/6J-129SvJ background (19) for over 11 generations and were housed in a temperature-controlled environment with a 12-h light/12-h dark cycle. Food intake and weights were determined daily, and all studies were performed on 12–14-week-old male mice. All animal protocols were performed in accordance with Albert Einstein College of Medicine of Yeshiva University IACUC (Institutional Animal Care and Use Committee) approval.

Indirect calorimetry. Metabolic measurement was performed using an Oxymax indirect calorimetry system (Columbus Instruments, Columbus, OH) (30). Mice were individually housed in the chamber with a 12-h light/12-h dark cycle in an ambient temperature of 22–24°C. VO_2 and VCO_2 rates were determined under Oxymax system settings as follows: air flow, 0.6 l/min;

From the [1]Department of Medicine and Molecular Pharmacology, The Albert Einstein College of Medicine, Bronx, New York; and the [2]Membrane Biology Laboratory, Institute of Molecular and Cell Biology, Singapore.

Corresponding author: Jeffrey E. Pessin, jeffrey.pessin@einstein.yu.edu.

Received 22 February 2010 and accepted 23 September 2010. Published ahead of print at http://diabetes.diabetesjournals.org on 28 September 2010. DOI: 10.2337/db10-0231.

sample flow, 0.5 l/min; settling time, 6 min; and measuring time, 3 min. The system was calibrated against a standard gas mixture to measure O_2 consumed (VO_2, ml/kg/h) and CO_2 generated (VCO_2, ml/kg/h). Metabolic rate (VO_2), respiratory quotient (ratio of VCO_2/VO_2), and activity (counts) were evaluated over a 24-h period. Energy expenditure was calculated as the product of the calorific value of oxygen ($3.815 + 1.232 \times$ respiratory quotient) and the volume of O_2 consumed.

In vivo assessment of insulin action and glucose metabolism. Five days before the experiment, the mice were anesthetized with ketamine (100 mg/kg) and xylazine (10 mg/kg), and two indwelling catheters with prefilled heparin (1,000 units/ml) and polyvidone–povidone (0.5 g/ml; Sigma) were introduced in the right internal jugular vein and left carotid artery. The catheters were externalized through an incision in the skin flap behind the head, and the mice were returned to individual cages after the surgery. The mice were fully recovered from the surgery before the in vivo experiments, as reflected by their reaching preoperative weight.

Euglycemic–hyperinsulinemic clamp. After a 12-h fast, euglycemic–hyperinsulinemic clamps were conducted in conscious mice as previously described (31,32) with minor modification. The 2-h euglycemic–hyperinsulinemic clamp was conducted with a continuous infusion of human insulin (4 mμ/kg/min) and a variable infusion of 25% glucose to maintain glucose at 90 mg/dl. Insulin-stimulated whole-body glucose metabolism was estimated using continuous infusion of [3-^{3}H]glucose (0.1 μCi/min; PerkinElmer Life Sciences). To determine the rate of basal glucose turnover, [3-^{3}H]glucose (0.05 μCi/min) was infused for 2 h (basal period) with 5 μCi bolus before starting the euglycemic–hyperinsulinemic clamp, and a blood sample was taken at the end of this basal period. To assess insulin-stimulated tissue-specific glucose uptake, 2-deoxy-*d*-[1-^{14}C]glucose 2-[^{14}C]DG (PerkinElmer Life Sciences) was administered as a bolus (10 μCi) 75 min after the start of the clamp. Blood samples were taken at time 0 and every 10 min from 80–120 min through the carotid artery. To estimate basal muscle glucose uptake, 2-[^{14}C]DG glucose was infused with isotonic saline. During the clamp, plasma glucose was monitored using 2 μl of blood by glucose meter (precision Xtra, Abbot, Bedford, MA). Plasma [3-^{3}H]glucose, 2-[^{14}C]DG glucose, and ^3H_2O concentration were measured as described previously (31). After the euglycemic–hyperinsulinemic clamp, individual tissue samples were collected and immediately frozen at −80°C for the measurement of glucose uptake.

Oral glucose tolerance test. Mice fasted for 12 h were administrated glucose (1g/kg) by oral gavage. Plasma samples were collect at 0, 30, 60, and 120 min for glucose and insulin levels. Glucose was measured using a glucose meter (precision Xtra, Abbot, Bedford, MA). Insulin levels were determined by ELISA (Crystal Chem Inc., Downers Grove, IL).

Dynamic glucose disposal. The stable isotope-labeled intraperitoneal glucose tolerance test (SipGTT) was performed as previously described (33). Briefly, male wild-type and VAMP8 null mice were overnight fasted and were given a 1.0 g/kg intraperitoneal injection of glucose (containing 50% [6,6-$^2H_2$]-glucose). The amount of the M+2 label in the C3–C6 fragment for [6,6-$^2H_2$]glucose was determined by electron impact ionization mass spectrometry, after conversion of the glucose to a glucose aldonitrile pentaacetate derivative (34).

Acute insulin stimulation. For acute insulin stimulation, the mice were fasted for 12 h and given either isotonic saline or human recombinant insulin (1U/kg) by intraperitoneal injection. Fifteen min later the animals were anesthetized with pentobarbital sodium (50 mg/kg), and tissue samples were collected and subjected to immunoblotting and immunofluorescence.

Immunoblotting. Tissues isolated from acute insulin stimulation were homogenized in ice-cold lysis buffer (50 mmol/l Tris, pH 7.5, 150 mmol/l NaCl, 1% Triton X-100, 1 mmol/l EDTA, 1 mmol/l phenylmethylsulfonyl fluoride, 0.25% sodium deoxycholate, 1 mmol/l NaF, 1 mmol/l Na_3VO_4, and 2 mmol/l $Na_4P_2O_7$) containing a protease inhibitor mixture (Roche Diagnostics). The resultant lysates were centrifuged at 16,000*g* for 60 min at 4°C, and protein concentrations were quantified using the bicinchoninic acid protein assays (Pierce). The protein samples (30 μg) were separated on a 4–12% gradient SDS-PAGE gel and transferred to nitrocellulose membranes using a semidry electroblotter (Owl Separation System, Portsmouth, NH). Membranes were immunoblotted with a VAMP8 polyclonal (18). Other antibodies were purchased from commercial suppliers: GLUT4 polyclonal antibody (East Acres Biologicals Inc.), GLUT1, -3, and -11 (Cell Signaling Technology, Inc.), UCP-1, UCP-2 (Abcam Inc.), and UCP-3 (Sigma). Quantification of all immunoblots was performed using NIH IMAGE software.

Immunofluorescence microscopy. Tissues isolated from acute insulin stimulation were embedded in optimal cutting temperature compound. The frozen tissue cross sections (10 μm) were blocked with 3% BSA in PBS for 60 min at room temperature. Primary antibodies were used at the following dilutions: GLUT4 polyclonal antibody (1:100) and α-dystroglycan (α-DG) antibody (1:50) as previously described (35). Fluorescently conjugated secondary antibodies (1:100, Jackson ImmunoResearch Laboratories) were added to the sections for 30 min at room temperature. After extensive washing with PBS, the slides were mounted with Vectashield Mounting Medium (Vector Laboratories). The slides were visualized by confocal fluorescent microscopy (model LSM510; Carl Zeiss MicroImaging, Inc.). Quantification of cell surface immunofluorescence was performed using NIH IMAGE software.

Statistical analysis. Results are presented as the means ± SEM. Statistical significance was determined using an unpaired two-tailed Student *t* test, with $P < 0.05$ considered significant.

RESULTS

VAMP8 null mice have reduced adiposity. To examine the metabolic phenotype of the VAMP8 null mice, we first determine total body weight, total water, and lean and fat mass of male VAMP8 null mice compared with wild-type controls by quantitative nuclear magnetic resonance noninvasive imaging (Fig. 1). The VAMP8 null mice had reduced total body weight with no statistically significant difference in lean mass or total water content compared with control mice. In contrast, there was a marked reduction in total fat mass (Fig. 1*A*). This occurred despite normal caloric intake during both the light and dark cycles, and if normalized for body weight the VAMP8 null mice in fact have an approximate 10% increase in food intake (Fig. 1*B*). These observed changes in fat mass were confirmed by tissue dissection that confirmed no significant difference in gastrocnemius muscle (Fig. 1*C*) or liver (Fig. 1*D*) weight but with a marked reduction in epididymal adipose tissue mass (Fig. 1*E*). The reduced adiposity resulted from a large reduction in adipocyte cell size as observed by histological imaging (supplementary Fig. 1, available in an online appendix at http://diabetes.diabetesjournals.org/cgi/content/full/db10-0231/DC1).

Because changes in adipocyte cell size have been correlated with changes in the secretion and plasma levels of different cytokines, we next determined the plasma levels of leptin, resistin, retinol binding protein 4 (RBP4), and adiponectin in the fasted state (Fig. 2). Consistent with reduced adipocyte cell size in the VAMP8 null mice, leptin and RBP4 levels were significantly decreased whereas adiponectin levels were somewhat increased. However, there was no significant difference in plasma resistin levels between the VAMP8 null and wild-type control mice.

VAMP8 null mice display increased energy expenditure and insulin sensitivity. Because the VAMP8 null mice have reduced adiposity despite equivalent or slightly enhanced daily caloric intake, we hypothesized that these mice would display increased energy expenditure. This speculation would be consistent with increased levels of adiponectin. To determine whole-body energy expenditure, wild-type and VAMP8 null mice were subjected to indirect calorimetry (Fig. 3). Oxygen consumption was increased during both the light and dark cycles, resulting in a total 24-h increase corresponding to a 40% increase in total energy expenditure (Fig. 3*A* and *B*). The increased energy expenditure was also apparent when corrected for lean body mass (supplementary Fig. 5). This increase in energy expenditure also occurred even though the VAMP8 null mice also displayed a decrease in locomotor activity during the dark cycle (Fig. 3*C*).

Because increased energy expenditure can result from mitochondrial uncoupling, we examined the expression of UCP-1/2/3 in skeletal muscle and adipose tissue (supplementary Fig. 2, available in an online appendix). There was no significant difference in UCP-1 protein levels between wild-type and VAMP8 null mice in brown adipose tissue,

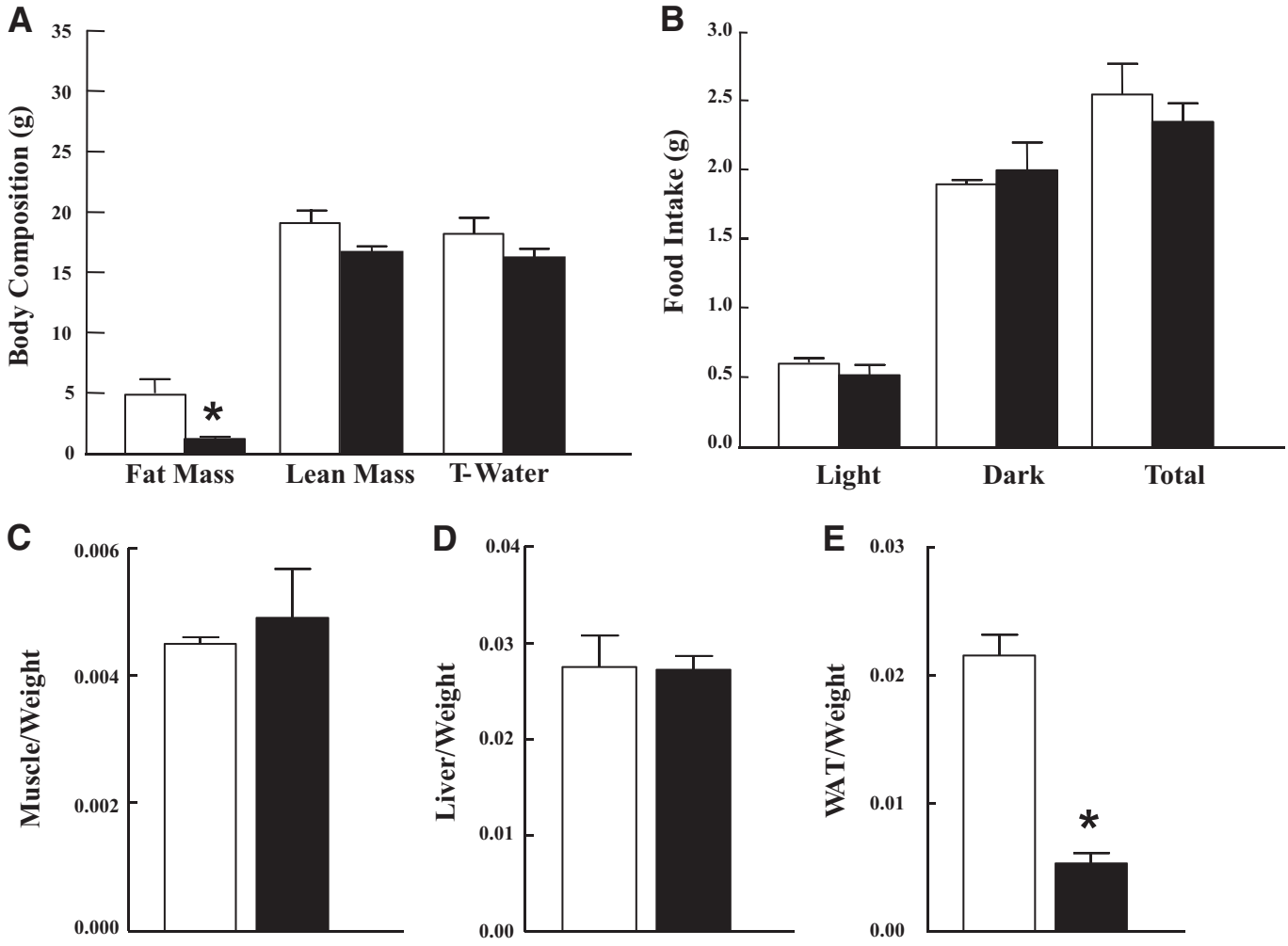

FIG. 1. VAMP8 null mice have a selective reduction in adipose tissue mass with normal food intake. *A*: Total adipose tissue and lean and water mass were determined in 12-week-old male wild-type (WT, open boxes) and VAMP8 null (VAMP8, filled boxes) mice by quantitative nuclear magnetic resonance. *B*: The average caloric intake of a normal chow diet during both the light and dark cycle was determined in an Oxymax open-circuit indirect calorimetry system over a 4-day period. *C*: Gastrocnemius skeletal muscle mass, (*D*) liver mass, and (*E*) epididymal adipose tissue mass per total body weight were determined by dissection and weighing of the individual tissues. These data represent the mean ± SEM from five individual mice per group. **P* < 0.05.

white adipose tissue, or red gastrocnemius skeletal muscle, although we were unable to detect UCP-1 protein in white gastrocnemius skeletal muscle. Similarly, there was no change in UCP-3 levels in any of the tissues examined. In contrast, UCP-2 protein levels were increased in white gastrocnemius skeletal muscle of the VAMP8 null mice with no change in white adipose tissue or red gastrocnemius skeletal muscle.

In any case, the increase in energy expenditure and reduced adiposity resulted in marked enhancement of glucose tolerance along with a decrease in fasting plasma glucose levels (Fig. 4*A*). Although insulin levels were

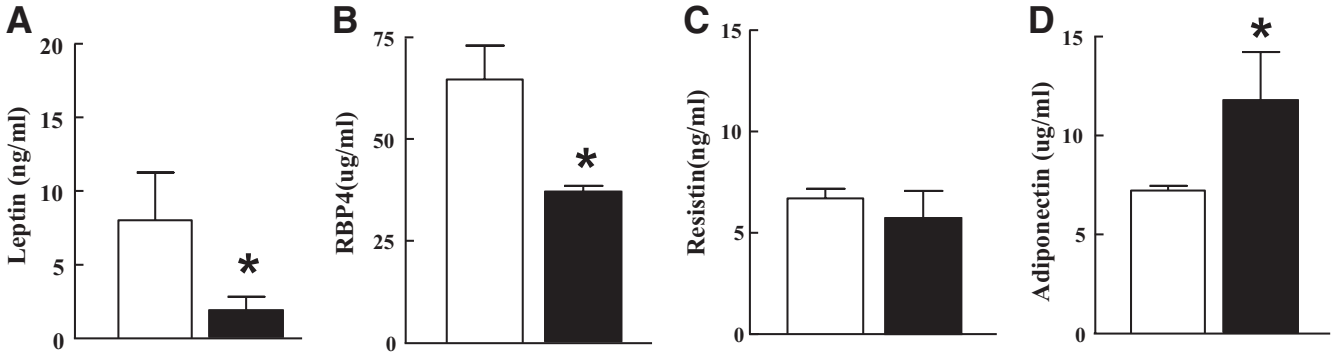

FIG. 2. VAMP8 null mice have changes in plasma levels of several adipokines. Fasting plasma levels of (*A*) leptin, (*B*) RBP4, (*C*) resistin, and (*D*) adiponectin in WT (open boxes) and VAMP8 (filled boxes) mice were determined by ELISA analysis. These data represent the mean ± SEM from six mice per group. **P* < 0.02.

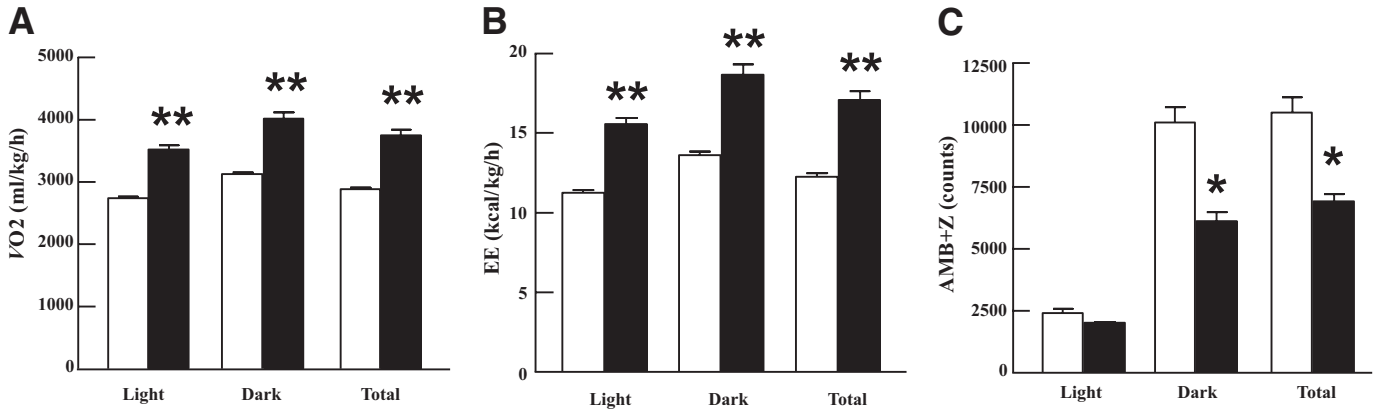

FIG. 3. Loss of VAMP8 expression results in increased energy expenditure (EE). Fourteen-week-old WT (open boxes) and VAMP8 (filled boxes) mice were placed into Oxymax open-circuit indirect calorimetry system over a 4-day period. The mice were fed in the 12-h dark cycle, and food was restricted during the 12-h light cycle. The average oxygen consumption in ml/kg/h (*A*) and energy expenditure in kcal/g/h (*B*) were determined. ***P* < 0.003. *C*: Spontaneous locomotor activity in the *x*, *y*, and *z* planes were determined as the total number of beam brakes. These are the averages from five WT and four VAMP8 mice. **P* < 0.05.

somewhat reduced in both the fasting state and during an oral glucose tolerance test, the changes in insulin levels paralleled the changes in plasma glucose, suggesting that total pancreatic β-cell insulin secretion was not significantly affected (Fig. 4*B*). Similarly, SipGTT demonstrated a greater clearance of glucose in the VAMP8 null mice compared with controls (Fig. 4*C*). Quantification of the area under the curve showed that the VAMP8 null mice display a reduction in glucose excursion, increased glucose disposal with a concomitant reduction in total insulin secretion levels (Fig. 4*D*).

To specifically determine whether the VAMP8 null mice

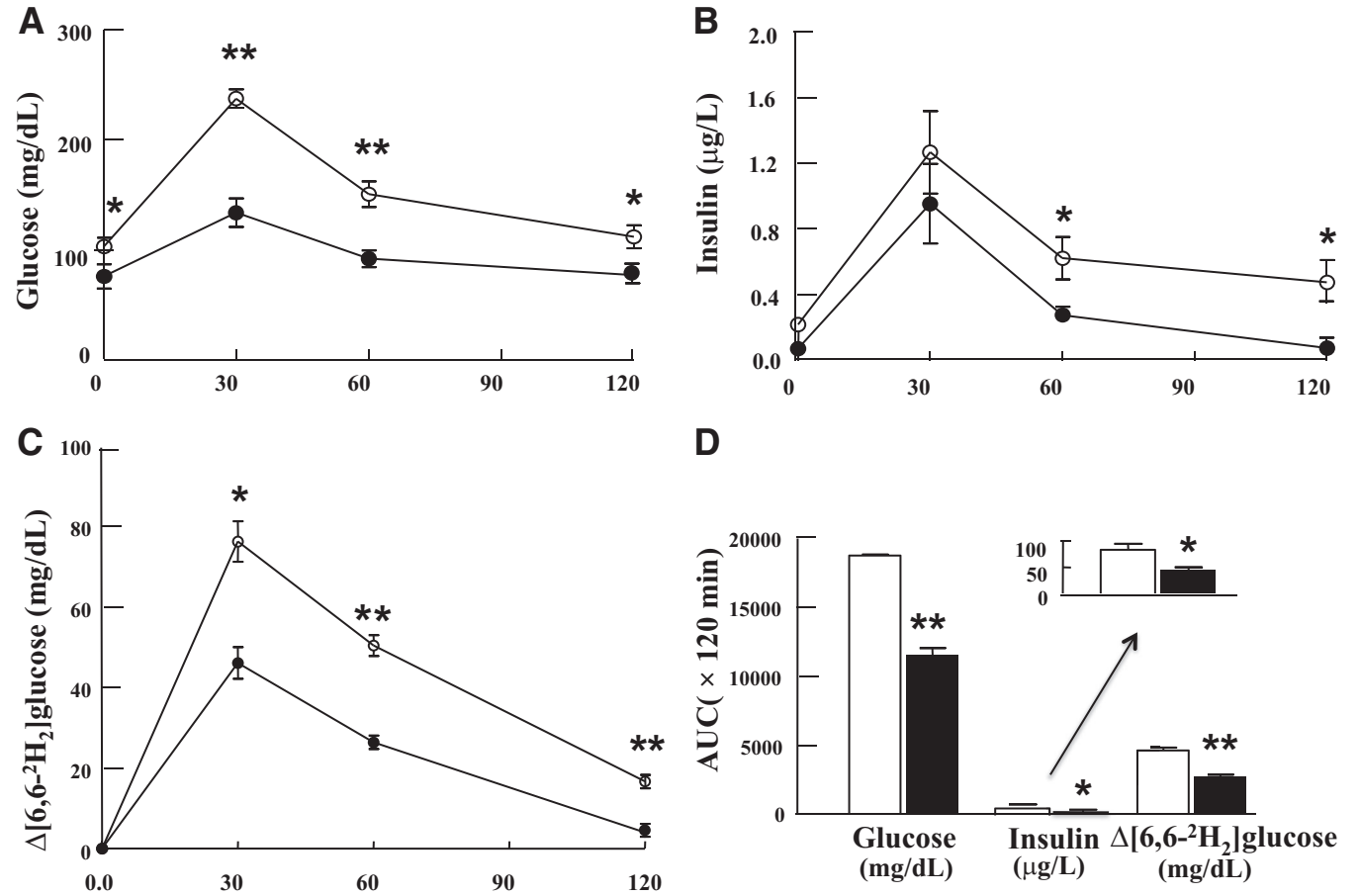

FIG. 4. VAMP8 mice display enhanced glucose tolerance. Twelve-week-old WT (open circles) and VAMP8 (filled circles) were fasted for 14 h and given 1 g/kg of D-glucose in isotonic saline by oral gavage. Blood (10 μl) was collected from the tail vein at 0, 30, 60, and 120 min. The blood glucose (*A*) and insulin (*B*) levels were determined and represent the mean ± SEM from five individual mice per group. **P* < 0.05, ***P* < 0.003. *C*: Twelve-week-old WT and VAMP8 mice were fasted for 15 h and given an intraperitoneal injection of 1g/kg of D-glucose 50% enriched with [6,6-$^2H_2$]-glucose. Each point represents the mean ± SEM from four individual mice per group. **P* < 0.05, ***P* < 0.001. *D*: The area under the curve for blood glucose and insulin levels were calculated from the glucose and glucose isotopomers measured during the SipGTT.

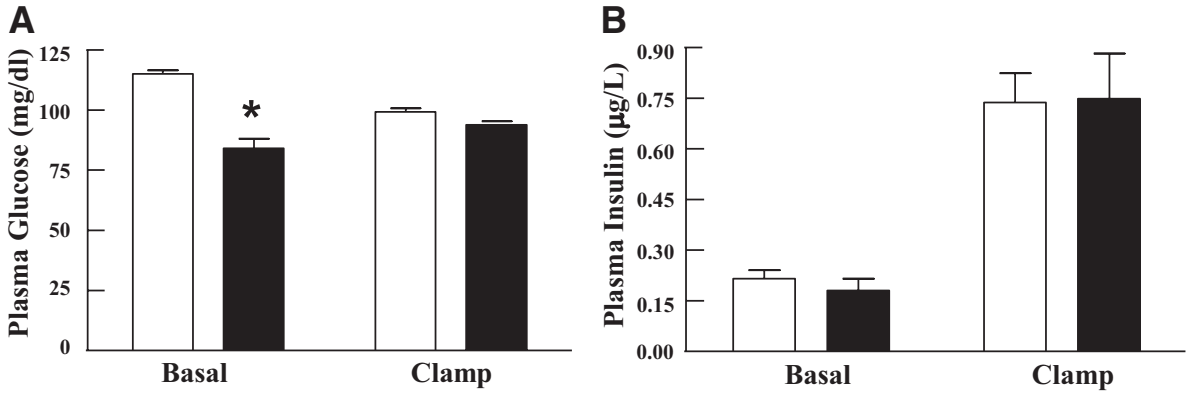

FIG. 5. Determination of plasma glucose and insulin levels during euglycemic–hyperinsulinemic clamps. *A*: Plasma glucose and (*B*) plasma insulin level during basal and last 30 min of the euglycemic–hyperinsulinemic clamps (4 mU/kg/min insulin infusion with glucose level maintained at ~90 mg/dl) for the WT (open boxes) and VAMP8 (filled boxes) mice. These data represent the mean ± SEM from 7–10 individual mice per group. *$P <$ 0.05.

display increased insulin sensitivity, we performed conscious nonstressed euglycemic–hyperinsulinemic clamps. As observed during the oral glucose tolerance test, in the basal or fasting level of plasma, glucose was reduced in the VAMP8 null mice compared with wild-type control and was normalized to the same level (~90 mg/dl) during the euglycemic–hyperinsulinemic clamp (Fig. 5*A*). Similarly, plasma insulin was normalized to the same hyperinsulinemic levels during the euglycemic–hyperinsulinemic clamp for both the wild-type and VAMP8 null mice (Fig. 5*B*). Consistent with an increase in insulin sensitivity, the glucose infusion rate during the euglycemic–hyperinsulinemic clamp was greater in the VAMP8 null mice along with increased whole-body glucose uptake (Fig. 6*A* and *B*). The overall rate of body glycogen/lipid synthesis was also increased with no statistically significantly change in total body glycolysis rate, although there was a consistent increased trend in the VAMP8 null mice (Fig. 6*C* and *D*). Skeletal muscle accounts for the majority of glucose postprandial glucose uptake and was significantly in-

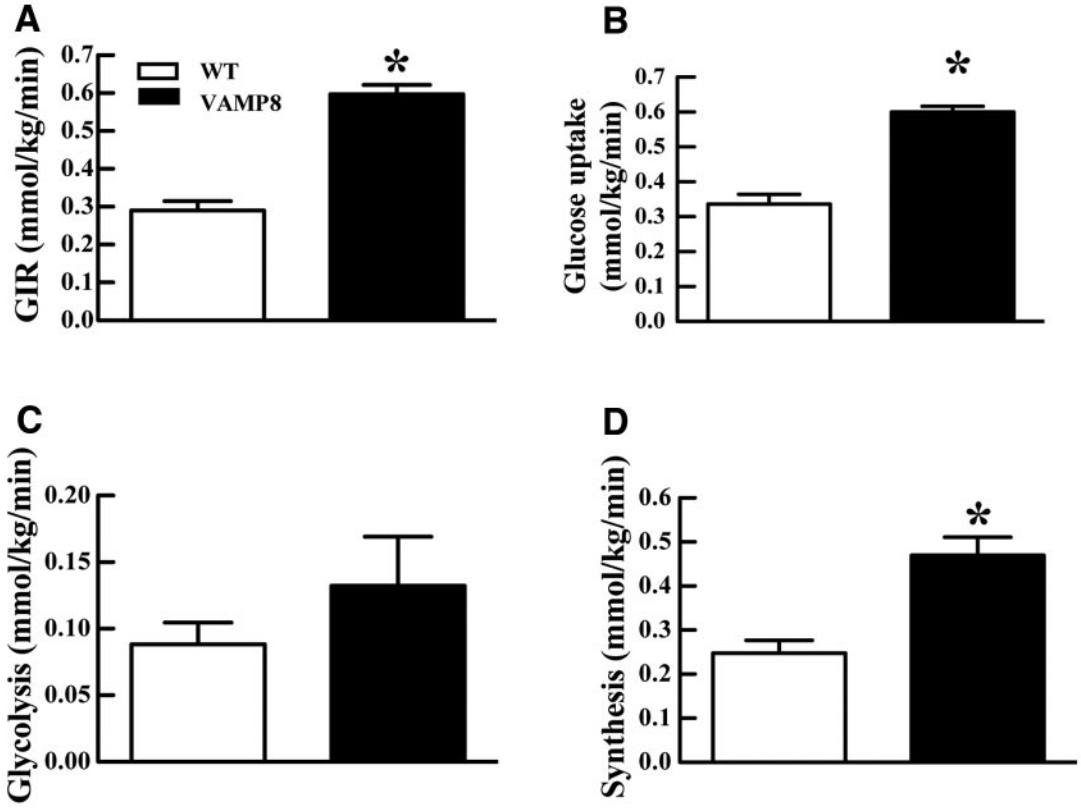

FIG. 6. VAMP8 mice have increased whole-body insulin sensitivity, glucose uptake, and glycogen/lipid synthesis. WT (open boxes) and VAMP8 (filled boxes) were subjected to euglycemic–hyperinsulinemic clamps to determine (*A*) the glucose infusion rate (GIR) necessary to maintain euglycemia. *B*: Whole-body glucose uptake was determined as [3-^{3}H]-glucose specific activity tracer infusion rate and weight of mice in the basal or euglycemic–hyperinsulinemic clamp state. *C*: The whole-body glycolysis was determined from the increment of the plasma ^3H_2O concentration multiplied by the estimated body water divided by [3-^{3}H]-glucose specific activity. *D*: The glycogen/lipid synthesis was estimated as the difference between whole-body glucose uptake and whole-body glycolysis. These data represent the mean ± SEM from 7–10 individual mice per group. *$P <$ 0.05.

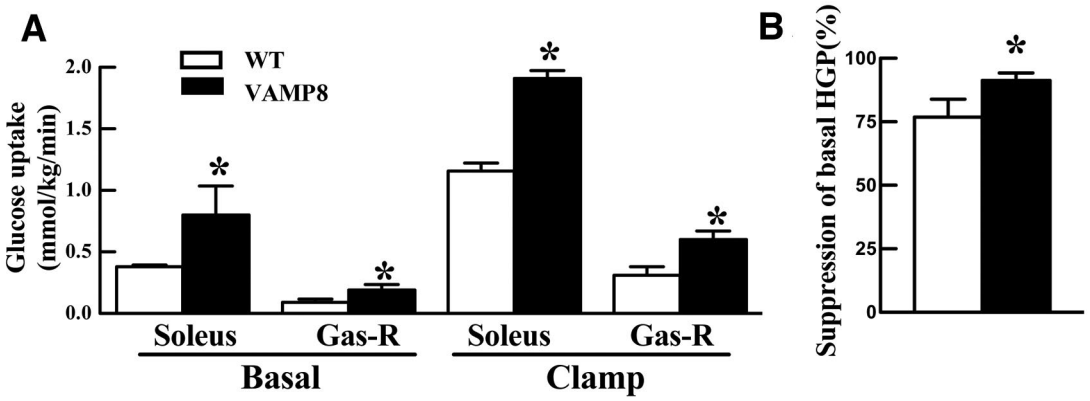

FIG. 7. VAMP8 mice have increased skeletal muscle glucose uptake with decreased hepatic glucose output (HGO). *A*: Basal and insulin-stimulated glucose uptake into skeletal muscle tissues (soleus and red gastrocnemius [GAS-R]) were determined by 2-deoxy-D-[1-^{14}C] glucose injection during the last 35 min of saline (basal) or insulin infusion during the euglycemic–hyperinsulinemic clamp. *B*: The insulin suppression of HGO was determined during the euglycemic–hyperinsulinemic clamp by [3-^{3}H]-glucose infusion. These data represent the mean ± SEM from 5–10 individual mice per group. *$P < 0.05$.

creased in red type 1 skeletal muscle fibers (soleus and red gastrocnemius) in both the basal and insulin-stimulated states (Fig. 7*A*). In parallel, insulin induced a greater suppression of hepatic glucose output in the VAMP8 null mice (Fig. 7*B*).

VAMP8 null mice have increased sarcolemma levels of glut4 protein. Because the VAMP8 null mice displayed increased insulin-stimulated glucose uptake and fasting hypoglycemia, we speculated that the sarcolemma distribution of GLUT4 might be increased. To examine this possibility, red gastrocnemius muscle from overnight-fasted wild-type and VAMP8 null mice were fixed and subjected to confocal immunofluorescence for the endogenous GLUT4 protein (Fig. 8*A*). The muscle fiber from the VAMP8 null mice displayed an increase in the cell surface distribution of GLUT4 as colocalized with the sarcolemma marker protein α-DG. The increased muscle cell surface distribution of GLUT4 in the VAMP8 null mice was even more pronounced in the insulin-stimulated state (Fig. 8*B*). Quantification of these data demonstrated a statistically significant increase in the sarcolemma GLUT4 protein of the VAMP8 null mice in the basal and insulin-stimulated states (Fig. 8*C*). Similar to that in the gastrocnemius muscle, confocal immunofluorescence of soleus muscle

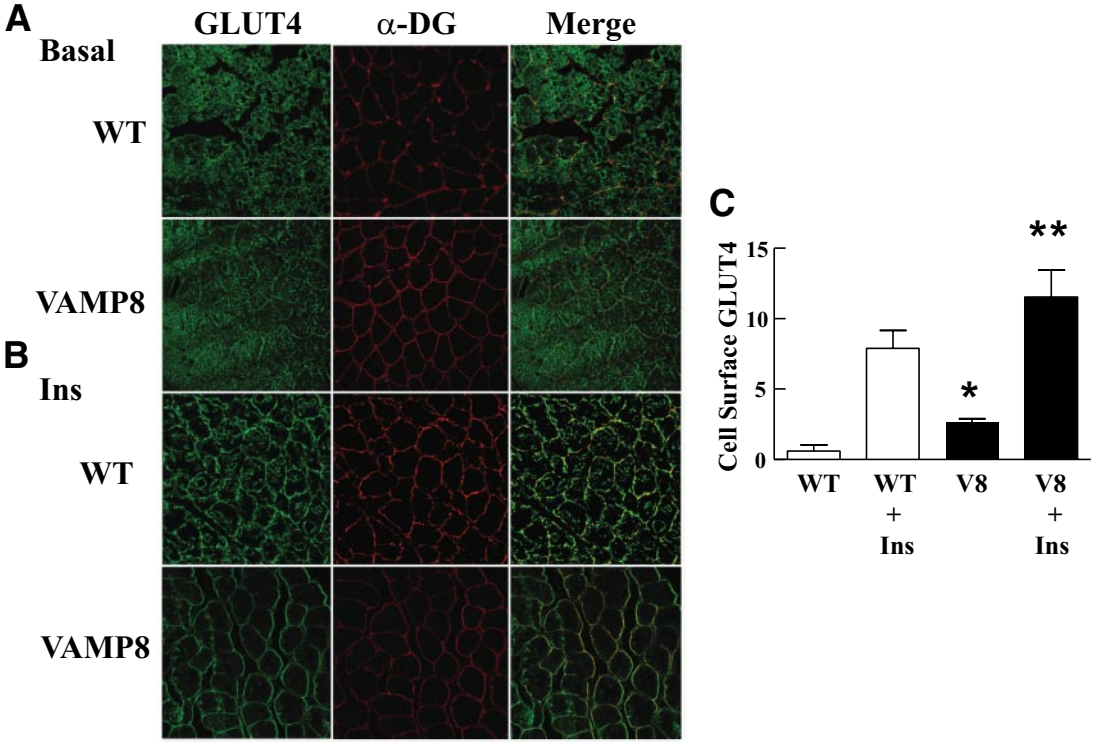

FIG. 8. VAMP8 (V8) mice have increased GLUT4 protein localized to the sarcolemma membrane in GAS-R skeletal muscle. WT and VAMP8 mice were fasted overnight (12 h) or given an intraperitoneal injection of either (*A*) isotonic saline or (*B*) insulin (Ins, 1 unit/kg). Fifteen min later, the GAS-R muscle was isolated and embedded in optimal cutting temperature compound as described in Research Design and Methods. The frozen tissue cross sections (10 μm) were then subjected to confocal immunofluorescence with specific GLUT4 and the α-DG antibody. Representative images are shown, and quantification of the relative extent of cell surface distribution of GLUT4 (*C*) was determined as the mean ± SEM from 5–10 independent mice. *$P < 0.05$, **$P < 0.003$, WT mice (open boxes), and VAMP8 mice (filled boxes). (A high-quality digital representation of this figure is available in the online issue.)

also demonstrated increased basal and insulin-stimulated sarcolemma GLUT4 localizations in the VAMP8 null mice compared with the control wild-type mice (supplementary Fig. 3, available in an online appendix). This change in GLUT4 subcellular distribution occurred with no significant change in the total expression levels of the GLUT4 protein or the total protein levels of several other facilitative glucose transporters GLUT1, GLUT3, and GLUT11 (supplementary Fig. 4, available in an online appendix).

DISCUSSION

Loss of VAMP8 protein levels results in the impairment of multiple distinct membrane-trafficking processes including the terminal membrane fusion event of cytokinesis, zymogen granule release in pancreatic acinar cells, degranulation of mast cells, transcytosis in polarized epithelial cells, secretory granule release from platelet and cytotoxic T-cells, and the plasma membrane exocytosis of the cystic fibrosis membrane conductance regulator and the aquaporin 2 water channel (21,23,25,26,28,29,36–41). In contrast, other studies have reported alternative roles for VAMP8 in membrane trafficking. For example, VAMP8 function is necessary for homotypic fusion of early and late endosomes, endosome–lysosome fusion, enhanced vesicle recycling between endocytic vesicles and the endosome in pancreatic β-cells, and GLUT4 endocytosis in adipocytes (15,17,20,21).

To examine the physiologic role of VAMP8 in glucose homeostasis in vivo, we took advantage of the VAMP8 null mice (19). Surprisingly, despite the alterations of different intracellular trafficking events, these mice displayed a marked reduction in adipocyte cell size with increased secretion levels of the adipokine adiponectin that favor enhanced glucose metabolism through increased fatty acid oxidation (42–45). More remarkably, the VAMP8 null mice have reduced spontaneous activity with identical caloric intake compared with the wild-type mice, yet rather than gaining adipose tissue mass, the VAMP8 null mice are leaner apparently due to increased total body energy expenditure. The increase in whole-body energy expenditure was not due to changes in adipose tissue or skeletal muscle UCP-1 or UCP-3 expression. Although UCP-3 is the predominant isoform present in skeletal muscle with lower levels of UCP-2 (46,47), we observed a significant increase in UCP-2 protein levels specifically in white gastrocnemius skeletal muscle of the VAMP2 null mice. Thus, it remains possible that the elevated UCP-2 levels account for the increase in energy expenditure, and the reduced size of adipocytes could result from an increased demand of skeletal muscle for fatty acid oxidation. Future studies will be necessary to directly assess this possibility and the mechanism responsible for the tissue-specific UCP-2 induction.

The enhanced metabolic balance of the VAMP8 null mice was also reflected in increased whole-body glucose tolerance and insulin sensitivity. Although there was a small enhancement in insulin suppression of hepatic glucose output, the major effect was a marked increase in skeletal muscle glucose uptake in both the basal and insulin-stimulated states. The increase in glucose uptake in the basal state is also consistent with the relative fasting hypoglycemia in the VAMP8 null compared with wild-type mice. Mechanistically, the loss of VAMP8 resulted in a greater distribution of the skeletal muscle GLUT4 protein at the sarcolemma membrane in the basal state that is consistent with the increase in basal glucose uptake. Similarly, the greater extent of insulin-stimulated GLUT4 translocation to the sarcolemma is also consistent with the increase in insulin-stimulated glucose uptake. The increase in cell surface GLUT4 levels occurred without any change in total GLUT4 protein levels. Thus, the loss of VAMP8 function could result in either an increase in the rate of GLUT4 exocytosis and/or a decrease in sarcolemma GLUT4 endocytosis. As we have previously observed that VAMP8 has no effect on GLUT4 exocytosis but is required for efficient GLUT4 endocytosis in 3T3L1 adipocytes (15), these data provide in vivo support for VAMP8 providing a necessary function in the cell surface endocytosis of the GLUT4 protein.

The glucose metabolic characteristics in the VAMP8 null mice are remarkably analogous to transgenic mice overexpressing the GLUT4 gene both in normal GLUT4 target tissues and specifically in skeletal muscle (48–51). In all these models, overexpression of GLUT4 resulted in increased cell surface levels of the GLUT4 protein that resulted in reduced fasting glycemia, increased skeletal muscle glycogen content, and improved glucose tolerance and insulin sensitivity in peripheral tissue. This enhanced glucose handling previously reported for GLUT4 transgenic mice parallels the same reduction in fasting glucose, increased glycogen synthesis, and increased insulin sensitivity and glucose tolerance observed in the VAMP8 null mice. Moreover, the reduction in insulin levels that follows the reduction in plasma glucose was accompanied by compensatory lipolysis that is also consistent with the reduction of adipocyte cell size observed in the VAMP8 null mice

Although all these metabolic data are consistent with VAMP8 playing a role in modulating skeletal muscle cell surface GLUT4 levels, how then do we also account for the observations that a variety of exocytotic secretory events are inhibited in VAMP8 null mice? One simple possibility is that VAMP8 plays different roles in the membrane trafficking of different cell types and/or for different cargo proteins. Alternatively, a more interesting possibility is the presence of a direct coupling between the endocytosis and exocytosis processes. Previously, it was reported that inhibition of chromaffin cell endocytosis by blocking dynamin function with a dynamin antibody resulted in a progressive decrease in catecholamine release (52). Similarly, blockade of dynamin function with a dominant-interfering mutant or reduction in dynamin protein levels by siRNA resulted in relatively normal initiation of first-phase secretion but that was subsequently inhibited along with the more prolonged inhibition of second-phase secretion in cultured β-cells (53). These data suggest the presence of a direct coupling between granule exocytosis (fusion pore opening) and endocytosis (fusion pore closure) events. Thus, another possibility is that the extent of membrane exocytosis is directly coupled to endocytosis in a manner necessary to prevent unrestricted expansion of the plasma membrane surface area. In this case, blockade of VAMP8 function also results in an inhibition of membrane exocytosis via a feedback mechanism arising from the prevention of normal membrane endocytosis and recycling.

In either case, the data presented demonstrate that the loss of VAMP8 expression has a marked effect on the integrative physiology of glucose metabolism and energy expenditure. These combined effects result in a leaner mouse with increased energy expenditure and glucose

disposal and insulin sensitivity. Thus, the development of a therapeutic strategy to inhibit VAMP8 function in skeletal muscle may be a viable approach to enhance glucose homeostasis.

ACKNOWLEDGMENTS

This study was supported by National Institutes of Health grants DK-033823, DK-082694, and DK-020541. No potential conflicts of interest relevant to this article were reported.

H.Z. performed experiments, contributed to discussion, and drafted the manuscript. C.-C.W., I.J.K., and W.H. contributed to discussion and reviewed and edited the manuscript. B.V. performed experiments, contributed to discussion, and reviewed and edited the manuscript. J.E.P. contributed to discussion and reviewed and edited the manuscript.

REFERENCES

1. Watson RT, Pessin JE. Intracellular organization of insulin signaling and GLUT4 translocation. Recent Prog Horm Res 2001;56:175–193
2. Holman GD, Sandoval IV. Moving the insulin-regulated glucose transporter GLUT4 into and out of storage. Trends Cell Biol 2001;11:173–179
3. Pessin JE, Thurmond DC, Elmendorf JS, Coker KJ, Okada S. Molecular basis of insulin-stimulated GLUT4 vesicle trafficking. Location! Location! Location! J Biol Chem 1999;274:2593–2596
4. Li D, Randhawa VK, Patel N, Hayashi M, Klip A. Hyperosmolarity reduces GLUT4 endocytosis and increases its exocytosis from a VAMP2-independent pool in l6 muscle cells. J Biol Chem 2001;276:22883–22891
5. Satoh S, Nishimura H, Clark AE, Kozka IJ, Vannucci SJ, Simpson IA, Quon MJ, Cushman SW, Holman GD. Use of bismannose photolabel to elucidate insulin-regulated GLUT4 subcellular trafficking kinetics in rat adipose cells. Evidence that exocytosis is a critical site of hormone action. J Biol Chem 1993;268:17820–17829
6. Fasshauer D. Structural insights into the SNARE mechanism. Biochim Biophys Acta 2003;1641:87–97
7. Weber T, Zemelman BV, McNew JA, Westermann B, Gmachl M, Parlati F, Söllner TH, Rothman JE. SNAREpins: minimal machinery for membrane fusion. Cell 1998;92:759–772
8. Sutton RB, Fasshauer D, Jahn R, Brunger AT. Crystal structure of a SNARE complex involved in synaptic exocytosis at 2.4 A resolution. Nature 1998;395:347–353
9. Bryant NJ, Govers R, James DE. Regulated transport of the glucose transporter GLUT4. Nat Rev Mol Cell Biol 2002;3:267–277
10. Duman JG, Forte JG. What is the role of SNARE proteins in membrane fusion? Am J Physiol Cell Physiol 2003;285:C237–249
11. Lin RC, Scheller RH. Mechanisms of synaptic vesicle exocytosis. Annu Rev Cell Dev Biol 2000;16:19–49
12. Rothman JE. Mechanisms of intracellular protein transport. Nature 1994; 372:55–63
13. Hong W. SNAREs and traffic. Biochim Biophys Acta 2005;1744:493–517
14. Rao SK, Huynh C, Proux-Gillardeaux V, Galli T, Andrews NW. Identification of SNAREs involved in synaptotagmin VII-regulated lysosomal exocytosis. J Biol Chem 2004;279:20471–20479
15. Williams D, Pessin JE. Mapping of R-SNARE function at distinct intracellular GLUT4 trafficking steps in adipocytes. J Cell Biol 2008;180:375–387
16. Zhao P, Yang L, Lopez JA, Fan J, Burchfield JG, Bai L, Hong W, Xu T, James DE. Variations in the requirement for v-SNAREs in GLUT4 trafficking in adipocytes. J Cell Sci 2009;122:3472–3480
17. Luzio JP, Pryor PR, Gray SR, Gratian MJ, Piper RC, Bright NA. Membrane traffic to and from lysosomes. Biochem Soc Symp 2005;72:77–86
18. Wong SH, Zhang T, Xu Y, Subramaniam VN, Griffiths G, Hong W. Endobrevin, a novel synaptobrevin/VAMP-like protein preferentially associated with the early endosome. Mol Biol Cell 1998;9:1549–1563
19. Wang CC, Ng CP, Lu L, Atlashkin V, Zhang W, Seet LF, Hong W. A role of VAMP8/endobrevin in regulated exocytosis of pancreatic acinar cells. Dev Cell 2004;7:359–371
20. Antonin W, Holroyd C, Tikkanen R, Höning S, Jahn R. The R-SNARE endobrevin/VAMP-8 mediates homotypic fusion of early endosomes and late endosomes. Mol Biol Cell 2000;11:3289–3298
21. Mullock BM, Smith CW, Ihrke G, Bright NA, Lindsay M, Parkinson EJ, Brooks DA, Parton RG, James DE, Luzio JP, Piper RC. Syntaxin 7 is localized to late endosome compartments, associates with Vamp 8, and Is required for late endosome-lysosome fusion. Mol Biol Cell 2000;11:3137–3153
22. Antonin W, Holroyd C, Fasshauer D, Pabst S, Von Mollard GF, Jahn R. A SNARE complex mediating fusion of late endosomes defines conserved properties of SNARE structure and function. EMBO J 2000;19:6453–6464
23. Bilan F, Nacfer M, Fresquet F, Norez C, Melin P, Martin-Berge A, Costa de Beauregard MA, Becq F, Kitzis A, Thoreau V. Endosomal SNARE proteins regulate CFTR activity and trafficking in epithelial cells. Exp Cell Res 2008;314:2199–2211
24. Tiwari N, Wang CC, Brochetta C, Ke G, Vita F, Qi Z, Rivera J, Soranzo MR, Zabucchi G, Hong W, Blank U. VAMP-8 segregates mast cell-preformed mediator exocytosis from cytokine trafficking pathways. Blood 2008;111: 3665–3674
25. Ren Q, Barber HK, Crawford GL, Karim ZA, Zhao C, Choi W, Wang CC, Hong W, Whiteheart SW. Endobrevin/VAMP-8 is the primary v-SNARE for the platelet release reaction. Mol Biol Cell 2007;18:24–33
26. Wang CC, Shi H, Guo K, Ng CP, Li J, Gan BQ, Chien Liew H, Leinonen J, Rajaniemi H, Zhou ZH, Zeng Q, Hong W. VAMP8/endobrevin as a general vesicular SNARE for regulated exocytosis of the exocrine system. Mol Biol Cell 2007;18:1056–1063
27. Puri N, Roche PA. Mast cells possess distinct secretory granule subsets whose exocytosis is regulated by different SNARE isoforms. Proc Natl Acad Sci U S A 2008;105:2580–2585
28. Sander LE, Frank SP, Bolat S, Blank U, Galli T, Bigalke H, Bischoff SC, Lorentz A. Vesicle associated membrane protein (VAMP)-7 and VAMP-8, but not VAMP-2 or VAMP-3, are required for activation-induced degranulation of mature human mast cells. Eur J Immunol 2008;38:855–863
29. Ho YH, Cai DT, Huang D, Wang CC, Wong SH. Caspases regulate VAMP-8 expression and phagocytosis in dendritic cells. Biochem Biophys Res Commun 2009;387:371–375
30. Xu J, Gowen L, Raphalides C, Hoyer KK, Weinger JG, Renard M, Troke JJ, Vaitheesyaran B, Lee WN, Saad MF, Sleeman MW, Teitell MA, Kurland IJ. Decreased hepatic futile cycling compensates for increased glucose disposal in the Pten heterodeficient mouse. Diabetes 2006;55:3372–3380
31. Zong H, Bastie CC, Xu J, Fassler R, Campbell KP, Kurland IJ, Pessin JE. Insulin resistance in striated muscle-specific integrin receptor beta1-deficient mice. J Biol Chem 2009;284:4679–4688
32. Ayala JE, Bracy DP, McGuinness OP, Wasserman DH. Considerations in the design of hyperinsulinemic-euglycemic clamps in the conscious mouse. Diabetes 2006;55:390–397
33. Vaitheesvaran B, Chueh FY, Xu J, Trujillo C, Saad MF, Lee WN, McGuinness OP, Kurland IJ. Advantages of dynamic "closed loop" stable isotope flux phenotyping over static "open loop" clamps in detecting silent genetic and dietary phenotypes. Metabolomics 2010;6:180–190
34. Xu J, Chang V, Joseph SB, Trujillo C, Bassilian S, Saad MF, Lee WN, Kurland IJ. Peroxisomal proliferator-activated receptor alpha deficiency diminishes insulin-responsiveness of gluconeogenic/glycolytic/pentose gene expression and substrate cycle flux. Endocrinology 2004;145:1087–1095
35. Kanagawa M, Michele DE, Satz JS, Barresi R, Kusano H, Sasaki T, Timpl R, Henry MD, Campbell KP. Disruption of perlecan binding and matrix assembly by post-translational or genetic disruption of dystroglycan function. FEBS Lett 2005;579:4792–4796
36. Pocard T, Le Bivic A, Galli T, Zurzolo C. Distinct v-SNAREs regulate direct and indirect apical delivery in polarized epithelial cells. J Cell Sci 2007; 120:3309–3320
37. Mukai A, Mizuno E, Kobayashi K, Matsumoto M, Nakayama KI, Kitamura N, Komada M. Dynamic regulation of ubiquitylation and deubiquitylation at the central spindle during cytokinesis. J Cell Sci 2008;121:1325–1333
38. Kanwar N, Fayyazi A, Backofen B, Nitsche M, Dressel R, von Mollard GF. Thymic alterations in mice deficient for the SNARE protein VAMP8/endobrevin. Cell Tissue Res 2008;334:227–242
39. Wang CC, Ng CP, Shi H, Liew HC, Guo K, Zeng Q, Hong W. A role for VAMP8/endobrevin in surface deployment of the water channel aquaporin 2. Mol Cell Biol 2010;30:333–343
40. Loo LS, Hwang LA, Ong YM, Tay HS, Wang CC, Hong W. A role for endobrevin/VAMP8 in CTL lytic granule exocytosis. Eur J Immunol 2009; 39:3520–3528
41. Kondkar AA, Bray MS, Leal SM, Nagalla S, Liu DJ, Jin Y, Dong JF, Ren Q, Whiteheart SW, Shaw C, Bray PF. VAMP8/endobrevin is overexpressed in hyperreactive human platelets: suggested role for platelet microRNA. J Thromb Haemost 2010;8:369–378
42. Yamauchi T, Kamon J, Minokoshi Y, Ito Y, Waki H, Uchida S, Yamashita S, Noda M, Kita S, Ueki K, Eto K, Akanuma Y, Froguel P, Foufelle F, Ferre P, Carling D, Kimura S, Nagai R, Kahn BB, Kadowaki T. Adiponectin stimulates glucose utilization and fatty-acid oxidation by activating AMP-activated protein kinase. Nat Med 2002;8:1288–1295

43. Mullen KL, Pritchard J, Ritchie I, Snook LA, Chabowski A, Bonen A, Wright D, Dyck DJ. Adiponectin resistance precedes the accumulation of skeletal muscle lipids and insulin resistance in high-fat-fed rats. Am J Physiol Regul Integr Comp Physiol 2009;296:R243–R251
44. Mullen KL, Smith AC, Junkin KA, Dyck DJ. Globular adiponectin resistance develops independently of impaired insulin-stimulated glucose transport in soleus muscle from high-fat-fed rats. Am J Physiol Endocrinol Metab 2007;293:E83–E90
45. Yamauchi T, Nio Y, Maki T, Kobayashi M, Takazawa T, Iwabu M, Okada-Iwabu M, Kawamoto S, Kubota N, Kubota T, Ito Y, Kamon J, Tsuchida A, Kumagai K, Kozono H, Hada Y, Ogata H, Tokuyama K, Tsunoda M, Ide T, Murakami K, Awazawa M, Takamoto I, Froguel P, Hara K, Tobe K, Nagai R, Ueki K, Kadowaki T. Targeted disruption of AdipoR1 and AdipoR2 causes abrogation of adiponectin binding and metabolic actions. Nat Med 2007;13:332–339
46. Boss O, Samec S, Dulloo A, Seydoux J, Muzzin P, Giacobino JP. Tissue-dependent upregulation of rat uncoupling protein-2 expression in response to fasting or cold. FEBS Lett 1997;412:111–114
47. Alán L, Smolková K, Kronusová E, Santorová J, Jezek P. Absolute levels of transcripts for mitochondrial uncoupling proteins UCP2, UCP3, UCP4, and UCP5 show different patterns in rat and mice tissues. J Bioenerg Biomembr 2009;41:71–78
48. Liu ML, Gibbs EM, McCoid SC, Milici AJ, Stukenbrok HA, McPherson RK, Treadway JL, Pessin JE. Transgenic mice expressing the human GLUT4/muscle-fat facilitative glucose transporter protein exhibit efficient glycemic control. Proc Natl Acad Sci U S A 1993;90:11346–11350
49. Treadway JL, Hargrove DM, Nardone NA, McPherson RK, Russo JF, Milici AJ, Stukenbrok HA, Gibbs EM, Stevenson RW, Pessin JE. Enhanced peripheral glucose utilization in transgenic mice expressing the human GLUT4 gene. J Biol Chem 1994;269:29956–29961
50. Ikemoto S, Thompson KS, Itakura H, Lane MD, Ezaki O. Expression of an insulin-responsive glucose transporter (GLUT4) minigene in transgenic mice: effect of exercise and role in glucose homeostasis. Proc Natl Acad Sci U S A 1995;92:865–869
51. Ren JM, Marshall BA, Mueckler MM, McCaleb M, Amatruda JM, Shulman GI. Overexpression of Glut4 protein in muscle increases basal and insulin-stimulated whole body glucose disposal in conscious mice. J Clin Invest 1995;95:429–432
52. Elhamdani A, Palfrey HC, Artalejo CR. Quantal size is dependent on stimulation frequency and calcium entry in calf chromaffin cells. Neuron 2001;31:819–830
53. Min L, Leung YM, Tomas A, Watson RT, Gaisano HY, Halban PA, Pessin JE, Hou JC. Dynamin is functionally coupled to insulin granule exocytosis. J Biol Chem 2007;282:33530–33536